algorithms

MDPI

Article

A New GIS-Based Detection Technique for Urban Heat Islands Using the Fuzzy C-Means Clustering Algorithm: A Case Study of Naples, (Italy)

Rosa Cafaro [1], Barbara Cardone [1], Valeria D'Ambrosio [1], Ferdinando Di Martino [1,2,*] and Vittorio Miraglia [1]

[1] Department of Architecture, University of Naples Federico II, Via Toledo 402, 80134 Napoli, Italy; rosa.cafaro@unina.it (R.C.); b.cardone@unina.it (B.C.); vdambros@unina.it (V.D.); vittorio.miraglia@unina.it (V.M.)
[2] Center for Interdepartmental Research "Alberto Calza Bini", University of Naples Federico II, Via Toledo 402, 80134 Napoli, Italy
* Correspondence: fdimarti@unina.it; Tel.: +39-081-2538904

Abstract: This study proposes a novel urban heat island detection method implemented in a GIS-based framework, designed to identify the most critical urban areas during heatwave events. The framework employs the fuzzy C-means clustering algorithm with remotely sensed land surface temperature and normalized difference vegetation index data to delineate and visualize hotspots. The proposed approach is compared with other established methods for urban heat island detection to evaluate their relative accuracy and effectiveness. This methodology integrates advanced spatial analysis with environmental indicators such as vegetation cover and permeable open spaces to assess urban vulnerability. The city of Naples, Italy, serves as a case study for testing the framework. The results from the case study indicate that the proposed method outperforms alternative methods in identifying heat hotspots, providing higher accuracy and suggesting potential adaptability to other urban contexts. This GIS-based approach not only provides a robust tool for urban climate assessment but also serves as a decision support framework that enables urban planners and policymakers to identify critical areas and prioritize interventions for climate adaptation and mitigation.

Keywords: UHI; heat island detection; FCM; GIS; urban vulnerability; climate adaptation

Academic Editors: Mateus Mendes, Balduíno Mateus, Nuno Lavado and Frank Werner

Received: 24 February 2025
Revised: 8 April 2025
Accepted: 11 April 2025
Published: 15 April 2025

Citation: Cafaro, R.; Cardone, B.; D'Ambrosio, V.; Di Martino, F.; Miraglia, V. A New GIS-Based Detection Technique for Urban Heat Islands Using the Fuzzy C-Means Clustering Algorithm: A Case Study of Naples, (Italy). *Algorithms* **2025**, *18*, 228. https://doi.org/10.3390/a18040228

1. Introduction

Urban heat islands (UHIs) are becoming an increasingly significant concern for urban environments and public health. These phenomena occur when urban surfaces such as asphalt and concrete absorb and retain heat, resulting in higher temperatures compared to surrounding peri-urban areas [1]. Excessive urban heat adversely impacts various dimensions of urban systems, intensifying energy consumption and thermal stress on both human and natural environments, with a decline in air and water quality [2,3]. As global cities continue to grow in size and population, it becomes increasingly important not to neglect the need for more accurate modeling and understanding of urban temperature dynamics and their consequences [4].

Much of the existing literature on UHIs focuses on temperatures variability—examining how temperature differences manifest seasonally or diurnally—and on assessing the public health implications associated with heat stress, heat-related illnesses, increased mortality, and elevated risks for vulnerable groups [5–7]. A further body of work explores how

high temperatures affect energy demands (e.g., building cooling needs) and investigates mitigation strategies, including changes to the built environment and the integration of green spaces. Understanding these spatial patterns is essential for informed urban planning, management, and climate resilience initiatives. Effective mitigation strategies depend on methods that precisely detect the spatial distribution of UHIs and analyze the conditions that contribute to them.

In the field of UHI analysis, two primary research approaches have been developed:

- Canopy-layer UHI analysis, in which a UHI is determined by measuring air temperatures, typically about 2 m above the ground level [8];
- Surface UHI (SUHI) analysis, in which a UHI is derived from remote sensing data [9].

While the first approach requires direct measurements of the air temperature above the ground, the second approach uses remotely sensed data on the thermal emissivity of the land surface to measure land surface temperatures (LSTs). Remote sensing data and above-ground air temperature measurements are not identical but are correlated [10–12]. In the literature, the two terms UHI and SUHI have become interchangeable in describing UHI patterns.

In this study, we refer to SUHI. It is important to highlight that remote sensing data offer greater spatial resolution and continuity compared to air temperature measurements. Air temperature data, typically collected by weather stations or in situ sensors, are often sparse and unevenly distributed [13], requiring interpolation techniques to estimate temperatures across broader areas. These interpolation processes, however, can introduce significant errors, especially in heterogeneous urban environments where microclimatic variations are pronounced. In contrast, satellite sensors provide consistent and high-resolution spatial coverage, capturing detailed thermal patterns across both urban and surrounding landscapes. This makes remote sensing a more reliable tool for characterizing the spatial dynamics of UHI.

Furthermore, unlike satellite-derived data, which offer consistent and globally accessible measurements, air temperature data collection varies by location, depending on the availability of monitoring infrastructure or specific survey campaigns. This variability complicates the transferability of UHI detection methodologies, potentially limiting their application in comparative studies across diverse urban settlements. Ensuring methodological consistency and minimizing dependence on localized data sources are therefore critical for enhancing the robustness and scalability of UHI detection frameworks.

Conventional UHI detection techniques involve a range of methods, including traditional classification methods such as threshold-based classification and spatial interpolation and advanced methods based on supervised machine learning (ML) or deep learning (DL) algorithms. Both approaches rely on remotely sensed datasets, such as LST raster data, and normalized difference vegetation index (NDVI) data obtained from satellite imagery (e.g., Landsat or MODIS), as well as meteorological data such as air temperature collected from ground stations or sensing campaigns. These techniques have several limitations that can impact their accuracy, scalability, and adaptability to different urban settlements. Machine learning (ML) and deep learning (DL) methods, while effective, depend on carefully labeled datasets, substantial computational resources, and expert knowledge. Moreover, data collection and management can be resource-intensive and error-prone, particularly in complex urban environments, limiting the scalability and efficiency of supervised techniques in UHI studies.

We propose an unsupervised UHI detection method based on the fuzzy C-means (FCM) fuzzy clustering algorithm. FCM is applied to detect urban heat islands from satellite-derived LST and NDVI data acquired during heatwaves. Additionally, the method assesses the spatial reliability of the detected urban heat islands based on the membership

degree of datapoints within the clusters. This represents an advantage over other methods, which do not allow for reliability estimation.

In response to the limitations of traditional methods, unsupervised AI-based UHI detection techniques offer a more detailed and adaptive approach to UHI detection. In addition, unlike AI-based supervised techniques, the proposed unsupervised UHI detection technique based on FCM does not require large, accurately labeled datasets, which are often difficult and costly to obtain. FCM identifies clusters directly from the data, assigning each data point a membership degree across multiple clusters. This flexibility allows the proposed FCM-based UHI detection method to better capture the continuous and heterogeneous nature of UHIs, providing a robust framework for accurately mapping and understanding UHI patterns.

Furthermore, to overcome the limitations of FCM in assigning the number of clusters a priori, the proposed method adopts a preprocessing phase in which validity indices such as Xie–Beni, Fukuyama–Sugeno, and Davies–Bouldin [14] are measured in order to determine the optimal number of clusters. These indices determine the optimal number of clusters by measuring the similarity between data points of each cluster and the dissimilarities between clusters.

Additionally, the proposed method has the advantage of estimating the reliability of the localization of the detected UHIs. This estimate is performed by measuring the average degree of belonging to the corresponding cluster of the data points that fall within the UHI. The higher this value is, within a range from 0 to 1, the more reliable the zoning and the extension of the detected UHI. This provides more detailed information for the decision maker to identify the urban areas most at risk during heat waves. This feature makes the proposed UHI detection method a robust and efficient tool for an accurate and reliable detection of urban heat islands.

In a nutshell, the proposed FCM-based UHI detection framework addresses key limitations of traditional supervised methods and offers unique advantages, including the following:

- Rather than being fixed a priori, the optimal number of clusters is determined using cluster validity indices. Their use allows for the assignment of the most appropriate number of clusters, ensuring that the result of the detection process accurately reflects the spatial patterns of UHIs.
- The unsupervised nature of FCM eliminates the need for extensive labeled datasets, significantly reducing computational requirements and preparation time compared to supervised methods.
- The flexibility of the proposed method allows it to adapt to various urban settings and dataset configurations, making it a versatile tool applicable across different geographical and environmental contexts. This feature, combined with the framework's ability to provide detailed information on the spatial distribution of UHI patterns, enables our method to provide valuable support for urban planners and policy makers in choosing targeted, nature-based heat resilience and heat mitigation solution strategies such as the implementation of green roofs and eco-streets, as well as enabling the evaluation of mitigation measures.

The proposed framework was tested on the metropolitan city of Naples, Italy, using land surface temperature (LST) and normalized difference vegetation Index (NDVI) datasets derived from Landsat 8. By clustering these datasets, our integrative approach provides a finer-resolution understanding of urban heat distribution, delivering refined precision in UHI mapping.

The paper is organized as follows: Section 2 explores the latest advancements in UHI detection using machine and deep learning methods, highlighting the shift from traditional

supervised approaches to unsupervised clustering techniques. Section 3 provides a brief overview of FCM and analyzes the validity indices employed to find the optimal number of clusters. Section 4 introduces the proposed framework and details its functional components. Section 5 presents and discusses the results of the tests executed on the case study. Finally, the conclusions are outlined in Section 6.

2. Related Work

Traditional approaches to UHI detection present significant limitations in practical applications. Direct methods of detection, such as composite thematic classifications of LST and NDVI or threshold-based approaches, often generate substantial errors at the urban scale due to the complex and heterogeneous nature of urban environments. These methods struggle to capture the subtle variations and transitions in thermal patterns that characterize urban landscapes.

More recent approaches to UHI detection employ supervised ML and DL algorithms. These techniques present significant limitations in practical application. The primary challenge lies in their dependency on extensive labeled training datasets, which require considerable time and resources to collect and validate.

Recent research has begun to explore the effectiveness of clustering techniques for identifying and mapping thermal patterns and hotspots, which are essential for informed decision-making in urban environment management [15]. This progress has been facilitated by the growing availability of high-resolution urban datasets [16] and unsupervised machine learning classification techniques, as highlighted by Lipson et al. [17]. These unsupervised methods do not require predefined labels, making them particularly suitable in contexts where satellite data labeling is complex and costly. Overall, these developments enable a transition to quantitative "bottom-up" approaches [18], demonstrating significant potential for more flexible and adaptable UHI detection by identifying complex thermal structures without manual supervision. Unsupervised learning methods have been applied to a few urban studies [19], for example to identify representative building groups and predict energy use at the city scale [20], to derive a detailed morphological classification of urban forms [21], and to identify typo-morphologies and perform thermal comfort simulations with Envi-met [22]. Other studies have utilized clustering techniques to investigate the surface urban heat island (SUHI) effect at the city scale [23]. In [24], a clustering-based methodology using the principal components analysis (PCA), agglomerative hierarchical clustering (AHC), and microclimate models, is tested to map urban heat island intensity at the territory scale to support urban planning. Another study [25] proposes an unsupervised learning approach based on Gaussian mixture models (GMMs), and GIS-data are used to map urban heat island intensity across the Canton of Geneva for urban planning purposes. The authors of [26] use k-means clustering to investigate the urban heat island effect in Duran, Ecuador, and propose mitigation strategies. In [27], Wang and Zhang introduce a functional zoning approach that utilizes weighted kernel K-means clustering to categorize urban functional zones based on thermal characteristics, thereby addressing the urban heat island phenomenon and informing urban planning and management strategies. A study by Doan et al. [28] introduces a novel clustering framework, S k-means, designed for mining spatiotemporal structured climate data. This framework enhances traditional k-means clustering by addressing the complexities inherent in climate data, such as high dimensionality and temporal variations. The ISODATA clustering method is used in [Cafaro et al., 2024] to detect urban heat islands in the city of Naples (Italy) by analyzing Landsat LST data acquired during heatwaves [29].

In Tehran, a fuzzy-based model was utilized to predict UHI locations by analyzing various contributing factors, achieving an accuracy of 78.6% in identifying high-risk areas [30].

In remote sensing, FCM is used for land use and land cover (LULC) mapping, enabling the differentiation of categories such as forests, agricultural fields, water bodies, and built-up areas [30]. It is particularly advantageous when analyzing regions with mixed pixels, where a single pixel represents multiple land cover types. By considering the membership degree, FCM enhances the accuracy of classification, especially in transitional zones or areas with gradual changes.

Additionally, FCM is employed for detecting environmental changes by segmenting satellite images captured at different times. This facilitates the monitoring of deforestation, urban expansion, and other dynamic processes [31]. In climate studies, FCM is used to identify areas with high pollution concentrations [32]. FCM has been used in healthcare to identify areas with high concentrations of disease cases (such as epidemics) where cluster boundaries are vague [33]. In the context of hotspot analysis, FCM can be used to identify areas with values significantly different from the average, such as regions with high crime, high traffic density, or fires.

Despite the many applications of FCM, its use in the analysis of UHIs remains an unexplored field. This study aims to demonstrate the effectiveness of this clustering algorithm in detecting UHIs, highlighting its several advantages over traditional detection methods commonly found in the literature. By integrating FCM within a GIS-based framework, our research introduces an innovative methodology for identifying UHI hotspots, providing urban stakeholders with a robust tool for implementing targeted measures to mitigate UHI effects and enhance urban resilience.

3. Preliminaries

In this section, the FCM algorithm is synthetized, and the validity indices used in our framework in the preprocessing phase to set the optimal number of fuzzy clusters are briefly described.

3.1. FCM Clustering

FCM [34,35] finds the cluster centers **V** and the partition matrix **U** that minimize the following objective function:

$$J(\mathbf{U},\mathbf{V}) = \sum_{i=1}^{C}\sum_{j=1}^{N} u_{ij}^{m} d_{ij}^{2} = \sum_{i=1}^{C}\sum_{j=1}^{N} u_{ij}^{m} \left\|\mathbf{x_j} - \mathbf{v_i}\right\|^2 \quad (1)$$

where $d_{ij} = \left\|\mathbf{x_j} - \mathbf{v_i}\right\|$ is the Euclidean distance between the center v_i of the ith cluster and the jth data point and $m \in [1,+\infty)$ is a parameter, called a fuzzifier, that defines the degree of fuzziness of the partition. For m = 1, FCM becomes a hard C-means clustering method; the more m trends towards $+\infty$, the more the fuzziness level of the clusters increases. An acceptable value for this parameter is m = 2.

The following constraints are respected:

$$\sum_{i=1}^{C} u_{ij} = 1 \; \forall \, j \in \{1,\ldots,N\} \quad (2)$$

$$0 < \sum_{j=1}^{N} u_{ij} < N \; \forall \, i \in \{1,\ldots,C\} \quad (3)$$

where Equation (2) states that the sum of the membership degrees of all clusters is equal to 1 and Equation (3) establishes that at least one data point must belong to a cluster with a non-zero membership degree and that the sum of the membership degrees of the data points in a cluster is less than the number of data points.

By applying the Lagrange multipliers to the Equation (1), the following solutions for **V** and **U** are obtained:

$$\mathbf{v}_i = \frac{\sum_{j=1}^{N} u_{ij}^m \mathbf{x}_j}{\sum_{j=1}^{N} u_{ij}^m} \qquad i \in \{1, ..., C\} \tag{4}$$

and

$$u_{ij} = \frac{1}{\sum_{k=1}^{c} \left(\frac{d_{ij}}{d_{kj}}\right)^{\frac{2}{m-1}}} \qquad i \in \{1, ..., C\},\ j \in \{1, ..., N\} \tag{5}$$

In [34,35], an iterative algorithm is proposed that allows for the minimization of the objective function (1), determining the solutions for **V** and **U**.

Initially, the C cluster centers are assigned randomly; at each iteration, the partition matrix is computed by (5), and the cluster centers are computed by (4). The algorithm stops after t iterations, when the following is true:

$$\left|\mathbf{U}^{(t)} - \mathbf{U}^{(t-1)}\right| < \varepsilon \qquad i = 1, \ldots, C; \qquad j = 1, \ldots, N \tag{6}$$

where $\varepsilon > 0$, called the end iteration threshold, is a parameter assigned a priori to terminate the algorithm if the maximum absolute difference between the partition matrix computed in the tth iteration and the previous partition matrix is below this threshold. In (6), this maximum absolute difference is given by the following:

$$\left|\mathbf{U}^{(t)} - \mathbf{U}^{(t-1)}\right| = \max_{\substack{i=1,...,C \\ j=1,...,N}} \left\{ \left| u_{ij}^{(t)} - u_{ij}^{(t-1)} \right| \right\} \quad i = 1, \ldots, C; \quad j = 1, \ldots, N \tag{7}$$

FCM has been used as a clustering algorithm in a wide range of applications and disciplines. It has the advantage of high computational speed, although it requires a priori fixing of the number of clusters.

In addition, different initializations can lead to different evolutions of the algorithm, which, in some cases, could converge to local minima. To overcome this limitation, it is possible to execute the algorithm multiple times.

Below is a pseudocode for the FCM algorithm (Algorithm 1).

Algorithm 1: FCM

Input: Original dataset with N points
Number of clusters C
Fuzzifier m
End iteration threshold ε

Output: The C segmented images

Initialize randomly the center of the clusters v_i i = 1, . . ., C
Repeat
  For i = 1, . . ., C
    For j = 1, . . ., N
      Compute u_{ij} by (5)
    Next j
    Compute v_i by (4)
  Next i
Until $\left|\mathbf{U}^{(t)} - \mathbf{U}^{(t-1)}\right| > \varepsilon$
Return V, U

3.2. Validity Indices

To ensure the robustness of the clustering results obtained from the FCM algorithm, various cluster validity indices are employed. These indices help in determining the optimal number of clusters by evaluating the quality of the clustering solution.

A cluster validity index is a numerical function of the number of clusters C; it measures the compactness of clusters and the separability between clusters. A cluster validity index is an effective method for determining the optimal number of clusters; its use does not require any a priori knowledge of the structure of the dataset. Generally, the optimal number of clusters C is determined as the value that maximizes or minimizes the index.

The following describes the three validity indices used in the proposed method, which are among those most widely adopted in fuzzy clustering: the Xie–Beni [36], Davies–Bouldin [37], and Fukuyama–Sugeno [38] indices. A complete discussion of the various validity indices proposed in the literature is provided in [39].

3.2.1. Xie–Beni Index (XBI)

The XBI is a popular fuzzy clustering validity measure proposed by Xie and Beni in [36]. It is defined as the ratio of compactness and separation, as shown in (8), where the sum of within-cluster squared distance, which is equivalent to the objective function J(**U**,**V**), divided by the total number of data points in the numerator is the compactness of the partition, and the minimum squared distance of cluster centers in the denominator is represents the separation.

$$\mathrm{XBI}(c) = \frac{\frac{1}{n}\sum_{i=1}^{c}\ \sum_{j=1}^{n}\ u_{ij}^{m}\left\|x_j - v_i\right\|^2}{\min\limits_{k\neq i}\left\|v_k - v_i\right\|^2} \tag{8}$$

where x_j, v_i, and v_k denote the jth object in the dataset and the ith and kth cluster centers, respectively; m is the fuzzifier; and u_{ij} is the membership degree of x_j to the ith cluster.

The smaller the numerator, the more compact the cluster, whereas the larger the denominator, the more the cluster is separated. Consequently, the smaller XBI, the better the partition. The optimal value C for the number of clusters is given by the value c for which XBI(c) is minimum. This is given by the following:

$$C = \underset{c}{\mathrm{argmin}}\,\mathrm{XBI}(c) \tag{9}$$

3.2.2. Davies–Bouldin Index (DBI)

This index evaluates the average similarity ratio between each cluster and its most similar cluster. A lower Davies–Bouldin index indicates better clustering performance, as it reflects greater separation between clusters. Computationally, the DBI requires several computations.

1. For each cluster C_i, calculate the average distance between each point in the cluster and the cluster centroid:

$$S_i = \frac{1}{|C_i|}\sum_{x\in C_i}\|x - c_i\| \tag{10}$$

where $|C_i|$ is the number of points in cluster C_i, x is a point in the cluster, and c_j is the centroid of C_j.

2. For each pair of clusters C_i and C_j, calculate the distance between their centroids:

$$M_{ij} = \left\|c_i - c_j\right\| \tag{11}$$

where c_i and c_j are the centroids of clusters C_i and C_j, respectively.

3. For each cluster C_i, calculate the similarity ratio with another cluster C_j. This ratio considers the intra-cluster distances and the inter-cluster distance:

$$R_{ij} = \frac{S_i + S_j}{M_{ij}} \tag{12}$$

4. For each cluster C_i, find the maximum similarity ratio R_{ij} with respect to all other clusters C_j. The DBI is then the average of these maximum values over all clusters:

$$DBI = \frac{1}{k} \max_{j \neq i} R_{ij}. \tag{13}$$

The optimal value C for the number of clusters is given by the value c for which XBI(c) is minimum; it is given by the following:

$$C = \arg\min_{c} DBI(c) \tag{14}$$

3.2.3. Fukuyama–Sugeno Index

This index combines the membership degree and the geometrical property of the dataset to evaluate a partition. It evaluates the quality of a clustering solution by measuring the discrepancy between the compactness and separation of clusters. The mathematical expression of FSI is given by the following:

$$FSI = \sum_{i=1}^{c} \sum_{j=1}^{n} u_{ij}^{m} \left\| x_j - v_i \right\|^2 - \sum_{i=1}^{c} \left(\sum_{j=1}^{n} u_{ij}^{m} \right) \| v_i - \overline{v} \|^2 \tag{15}$$

where the sum of within-cluster variances, as the first item in the equation, represents compactness, while the sum of squared distances between each cluster center and the mean of all cluster centers, as the second item in the equation, measures the separation pf partition. The term $\bar{v} = \frac{1}{c} \sum_{i=1}^{c} v_i$ is the center of gravity of the centroids of the C clusters.

Obviously, a smaller FSI indicates better performance of clustering. This is given by the following:

$$C = \arg\min_{c} FSI(c) \tag{16}$$

By utilizing these validity indices, FCM can automatically determine the most appropriate number of clusters for the dataset, enhancing the accuracy of UHI detection. This automated process reduces the need for subjective decision-making in cluster selection, making the methodology more efficient and applicable across various urban settlements.

4. The Proposed Framework

4.1. The Methodological Framework

The methodological framework developed for the identification and analysis of UHIs involves a systematic sequence of steps, as illustrated in the flow diagram in Figure 1.

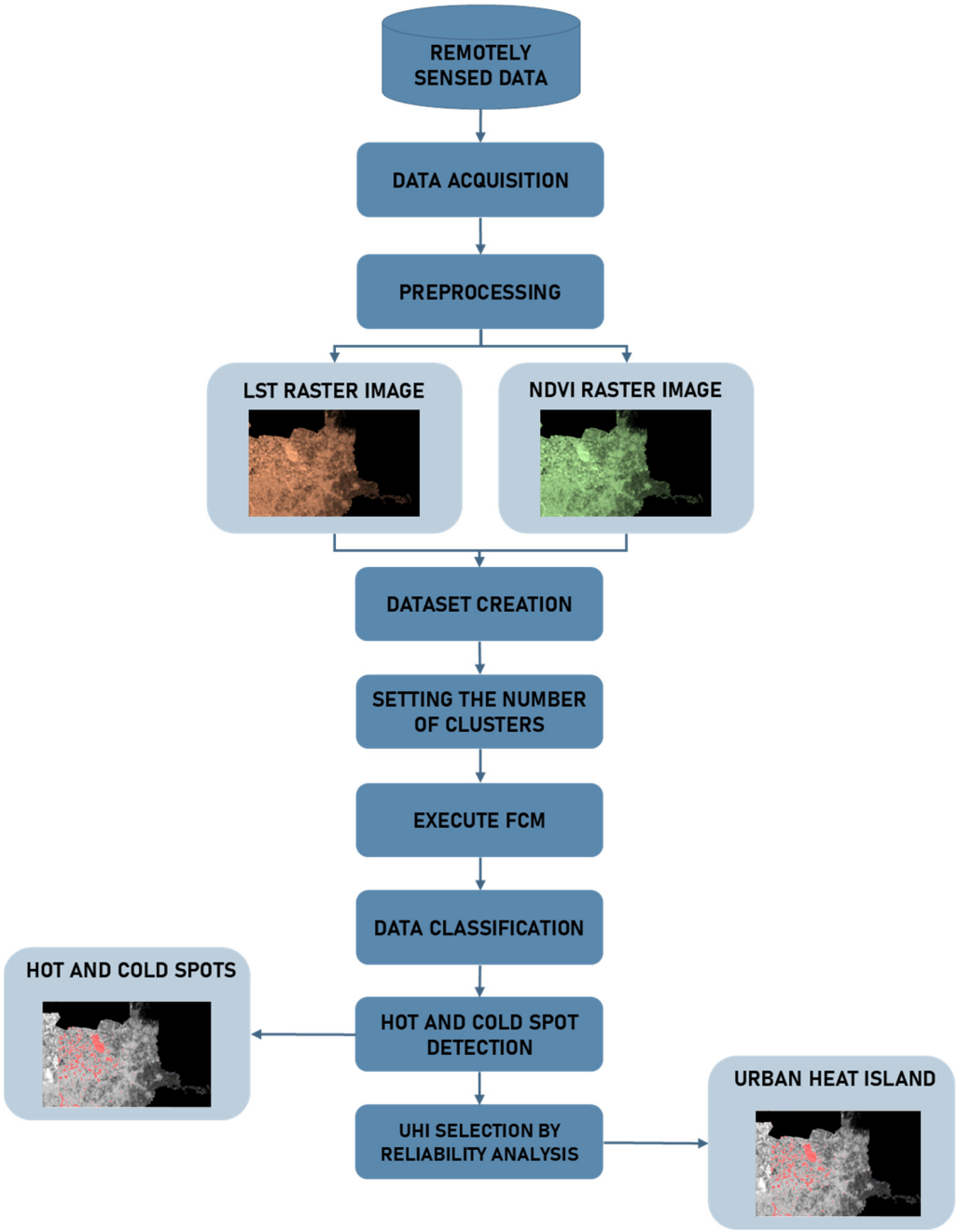

Figure 1. Flowchart of the model.

Below, the steps of the flowchart are described.

4.1.1. Data Acquisition

The initial step involves acquiring high-resolution geospatial data. Landsat 8 imagery is selected due to its 30 m × 30 m spatial resolution, which balances detailed urban analysis with manageable computational requirements. Two critical datasets are derived from this imagery:

- Land surface temperature (LST): LST data are extracted from the Thermal Infrared Sensor (TIRS) bands of Landsat 8. These bands capture thermal radiation, which is then converted into surface temperature values using the split-window algorithm. LST serves as the primary indicator of urban heat intensity.
- Normalized difference vegetation index (NDVI): The NDVI is calculated from the near infrared (NIR) and red bands of Landsat 8. This index measures vegetation density,

providing insight into the cooling effect of green spaces in urban areas. NDVI is essential for understanding the interplay between vegetation cover and heat distribution.

The acquisition process also includes quality checks to filter out poor-quality imagery, such as those affected by cloud cover or extreme atmospheric conditions, ensuring reliable inputs for subsequent analyses. The selection of satellite images for the heatwave period is carried out by analyzing heatwave periods according to the bulletin of the Italian Ministry of Health.

4.1.2. Preprocessing

The datasets (LST and NDVI) were then subjected to geometric correction operations to eliminate distortions caused by satellite acquisition or instrumentation errors and ensure that all data share the same projection coordinate system. This allowed for a consistent overlay of geospatial information. Once prepared and corrected, the dataset was subjected to a resampling process to obtain a uniform resolution of 30 m $\times$ 30 m, thus facilitating a correct comparison of the data without discrepancies related to different spatial resolutions. This step is crucial for maintaining consistency across the datasets, allowing for accurate integration and analysis of LST and NDVI values.

4.1.3. Dataset Creation and Setting the Number of Clusters

Each raster cell, now containing both LST and NDVI values, is treated as a multidimensional data point. This integration enables the FCM algorithm to simultaneously analyze the relationship between temperature and vegetation density.

A crucial aspect of running FCM is identifying the optimal number of clusters. The study utilizes various validity indices, including the Xie–Beni, Fukuyama–Sugeno, and Davies–Bouldin indices, to determine the optimal number of clusters (C). This step is vital for ensuring that the clustering results are meaningful and accurately reflect the underlying data patterns. The use of validity indices represents one of the innovative aspects of our method, as in other clustering approaches, the choice of the number of clusters is often arbitrary and made a priori, which may not accurately capture the nature of the data.

After a careful analysis of the scientific literature, it was observed in [38] that the validity indices used in this study, including Xie–Beni, Fukuyama–Sugeno, and Davies–Bouldin, are among the most applied in the context of the fuzzy C-means algorithm.

This alignment with established practices not only reinforces the robustness of the methodology but also enhances the credibility of the results, as these indices have been shown to effectively evaluate clustering performance in various contexts.

4.1.4. Execute FCM

After creating the dataset, the FCM algorithm is executed using the optimal number of clusters determined in the previous step.

As a result of the FCM algorithm, a classified raster image is generated, visually representing distinct thermal and vegetation patterns across the urban landscape. Each pixel in the raster is assigned to a cluster based on its maximum membership degree, ensuring a clear spatial representation of the different identified areas.

4.1.5. Data Classification and Hotspot Detection

A plot of the clusters' centroids is made after each pixel has been identified with the cluster to which it belongs. This allows for the identification of two thresholds, called hot and cold thresholds, which, respectively, are used to identify the hot and cold spots in urban zones, which are defined by high LST and low NDVI and low LST and high NDVI.

In the graph, the abscissa shows the LST, and the ordinate represents the NDVI.

The hot threshold identifies a point on the curve beyond which there is no significant change in NDVI as the LST increases.

The cold threshold identifies a point on the curve before which there is no significant change in the NDVI as the LST increases.

The plot in Figure 2 is an example of a trend in the NDVI with respect to the LST. Initially, the NDVI does not vary significantly with increasing LST; beyond the cold threshold point, the NDVI decreases exponentially with increasing LST, up to the hot threshold point, beyond which the curve shows a plateau, and the NDVI does not vary significantly with increasing LST.

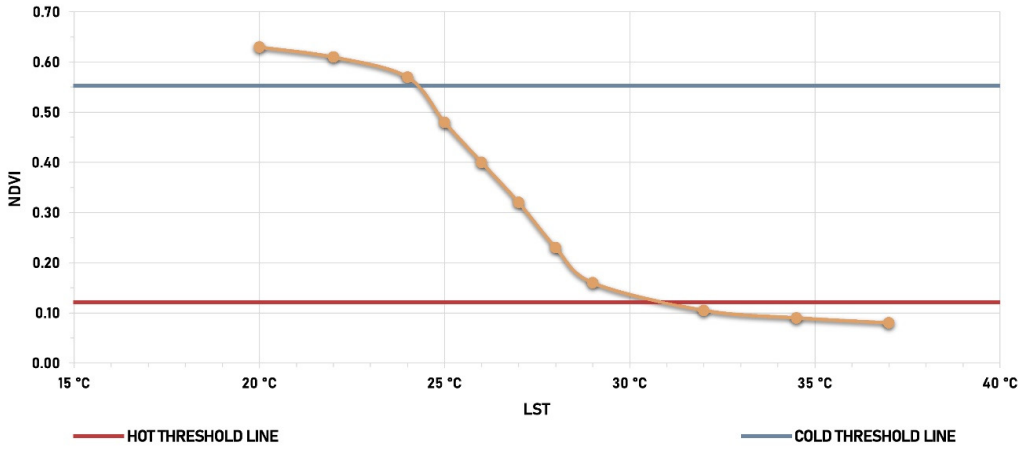

Figure 2. Example of a centroid Cartesian plot: LST vs. NDVI.

The two lines in Figure 2, labeled hot threshold line and cold threshold line, are the two horizontal lines intersecting the curve in the hot and cold spot points, respectively.

Once the centroids are plotted, a slope analysis is performed between adjacent centroids in order to fix the two thresholds.

Slope is a measure of the change in one value relative to another. In the context of centroid analysis, slope is calculated between adjacent centroids and represents the change in LST and NDVI values. A steep slope indicates a rapid and significant change in values, while a gentler slope suggests a more gradual change.

An area with a steep slope could indicate a transition from an area with high vegetation and low temperatures to an area with low vegetation and high temperatures. These transitions can be indicative of phenomena such as UHIs, where temperatures increase dramatically due to the lack of vegetation and the presence of artificial surfaces.

The two thresholds are fixed based on the value of the slope. The cold threshold is set as the point on the curve beyond which the slope increases to more than 10%. Likewise, the hot threshold is set as the point on the curve beyond which the slope definitively decreases to below 10%.

To set the threshold values, a preprocessing activity was performed in which, by varying these values, the corresponding hot and cold spots were detected, and their average reliability was measured. The threshold values of hot and cold spots equal to the points on the curve beyond which (below which) the slope decreases (increases) by 10% are those that provided the highest average reliability.

Furthermore, the resulting hot and cold spots were compared with a high-resolution digital orthophoto. This comparison was performed by observing that the detected hotspots corresponded on the digital orthophoto to predominantly impermeable areas with high building density and/or no vegetation and that the cold spots corresponded to areas predominantly with vegetal cover.

After selecting the two thresholds in the plot, the urban area hotspots are generated by aggregating neighboring pixels belonging to clusters having centroids beyond the hot threshold. Similarly, cold spots are generated by aggregating neighboring pixels belonging to clusters having centroids before the cold threshold.

4.1.6. UHI Selection by Reliability Analysis

In order to evaluate the reliability of an urban hotspot and identify it as a UHI, a reliability index is measured that is connected to the uncertainty of the membership of the pixels that compose the hotspot, where the uncertainty of the membership of a pixel to a cluster is given by its membership degree to that cluster.

This measure is obtained using a zonal statistical functionality that provides, for each hotspot polygon, the average value of the membership degrees to its own clusters of the pixels that compose it.

Formally, if the hth hotspot is obtained by aggregating N_h pixels and u_j is the membership degree of the jth pixel to the cluster to which it is assigned, the reliability of the hotspot is given by the following:

$$rel_h = \frac{1}{N_h} \sum_{j=1}^{N_h} u_j \tag{17}$$

This reliability index allows us to analyze the uncertainty and reliability of hotspots.

Finally, each urban hotspot is identified as a UHI and is assigned a reliability level. The reliability measure provides an estimate of how reliable the hotspot identification is as a UHI. Hotspots with reliability values higher than 75% are UHIs with a high degree of certainty; hotspots with reliability levels lower than 50% may represent areas with different urban and morphological characteristics that influence the surface behavior; they may be potential UHIs, but an in-depth urban scale analysis is needed to understand the behavior of the urban surface during heatwaves in these areas.

4.2. The Case Study

The experiment was conducted in the urban context of the city of Naples, Italy, as shown in Figure 3, due to its characteristics of high population density and building intensification.

Naples is characterized by a relatively small territorial surface, equal to 11,727 hectares, and a high population density, with approximately 8566 inhabitants per square kilometer. The metropolitan area of the city has a population of 295,700 inhabitants; of these inhabitants, those residing in the municipality of Naples amount to 1,004,500 inhabitants.

The city's climate is subtropical, slightly continental, and humid–subhumid with the near absence of intermediate seasons, featuring increasingly intense rain showers interspersed with long periods of drought.

In recent years the city has seen an increase in the frequency of heat waves lasting more than a few days throughout the summer months.

In many areas of the historic center and in recently developed areas, the expansion of concrete and asphalt surfaces has exacerbated the risk of thermal accumulation phenomena during the summer months, a phenomenon that has intensified in recent years due to the increasing frequency and duration of heat waves. The city center is characterized by a particularly high concentration of building and population density, with a significant prevalence of impermeable surfaces, to the detriment of the presence of urban green areas. On the contrary, the western and northwestern areas of the city are characterized by a greater diffusion of forest-type green areas, compared to the rest of the urban fabric. The eastern peripheral districts are predominantly intended for industrial uses, featuring a high building density along the coastal strip and a predominance of impermeable surfaces.

Figure 3. Study area of Naples, Italy.

The input data necessary for UHI hotspot detection consist of LST and NDVI raster datasets, both derived from remotely sensed imagery captured by the Landsat 8 satellite. These datasets were acquired on 30 July 2022, coinciding with a recorded heatwave event lasting 28 consecutive days, from 15 July to 11 August 2022. This ensures that the analysis is representative of extreme urban warming conditions. The imagery is publicly accessible through the USGS Earth Explorer platform.

The LST raster, derived from the Thermal Infrared Sensor (TIRS) bands (bands 10 and 11), which measure surface thermal radiation, exhibits temperature values ranging from a minimum of 28 °C to a maximum of 56 °C; it is shown in Figure 4.

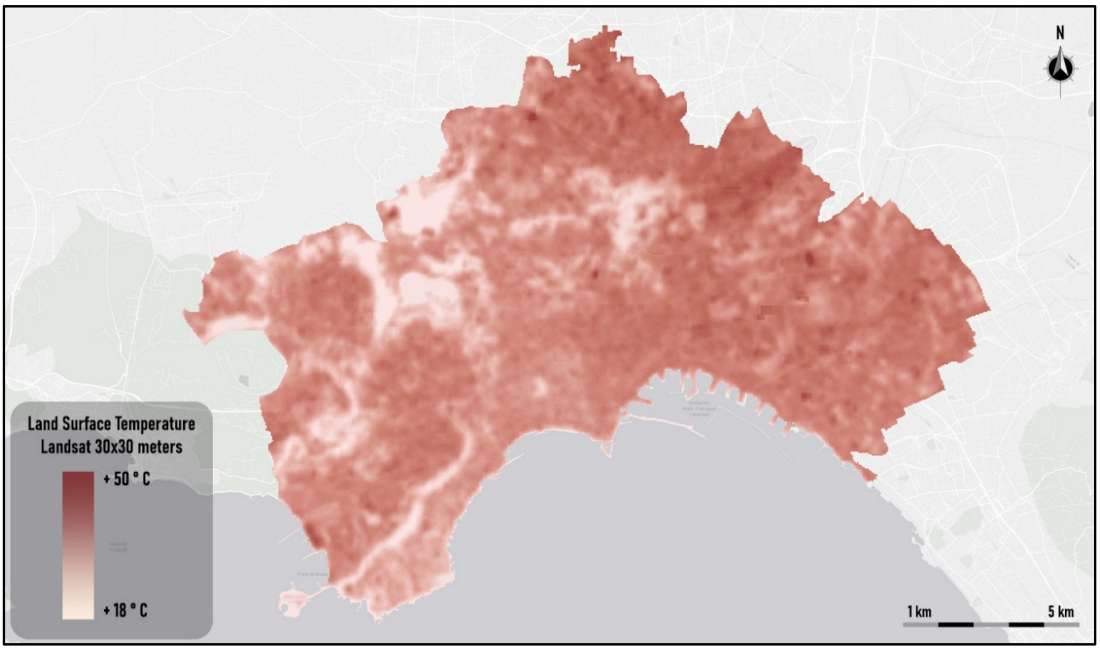

Figure 4. LST of the study area.

The NDVI raster, derived from the spectral bands of the Landsat Operational Land Imager (OLI) with a domain between −1 and +1, records values ranging from a minimum of −0.16 to a maximum of +1; it is shown in Figure 5. The NDVI raster was processed to match the spatial resolution of the LST dataset, ensuring accurate data integration for subsequent analysis.

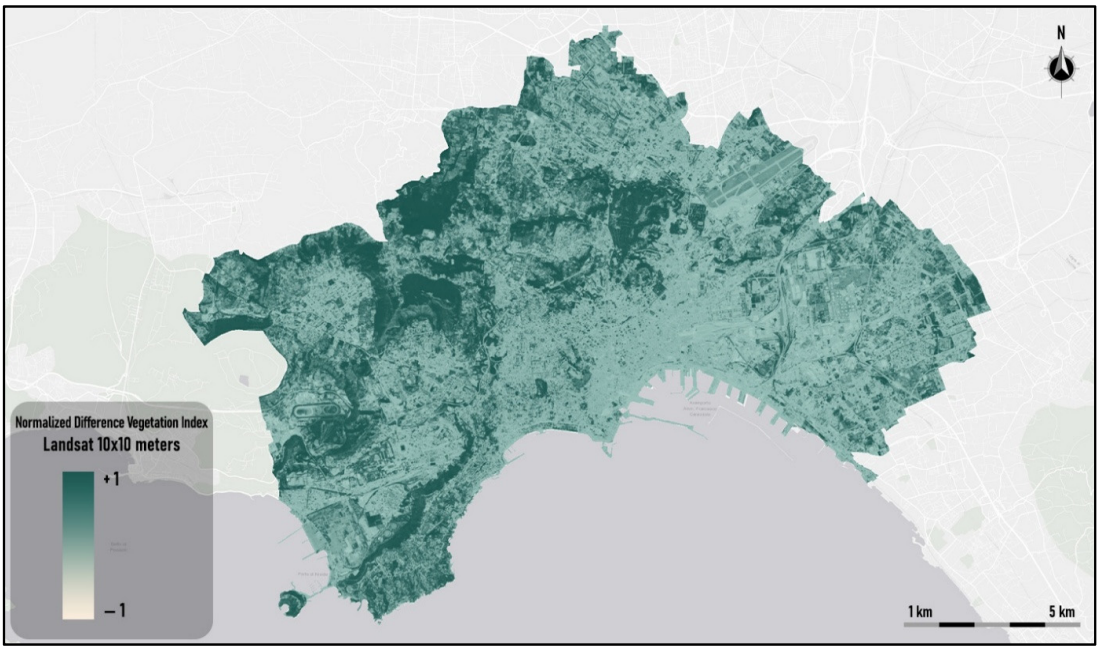

Figure 5. NDVI of the study area.

The two raster datasets represent the input data for the execution of the FCM clustering algorithm. The results and thematic maps of hotspot detection are shown in the following subsection.

Following the calculation of the validity indices, it emerged that the optimal number of clusters is equal to 9. The plot graph of the trend of NDVI with respect to LST is shown in Figure 6, where the two threshold lines are plotted; the hotspots are obtained by dissolving adjoining pixels belonging to clusters 3, 4, and 6. The cold spots are obtained by dissolving adjoining pixels belonging to clusters 8, 1, and 9.

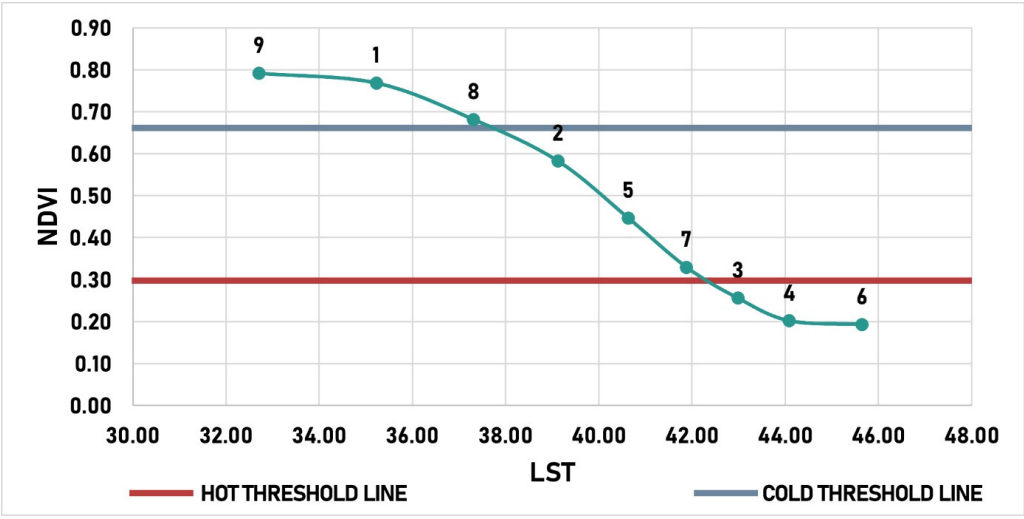

Figure 6. Centroid Cartesian plot: LST vs. NDVI.

The model was implemented on a GIS platform built using the ESRI ArcGIS Pro 3.4 Suite. Preprocessing, clustering, and fuzzy reliability calculations were performed using ESRI ArcPy Python libraries for ArcGIS Pro 3.4, in which the FCM algorithm was implemented.

5. Results and Discussion

5.1. UHIs Detected

The clusters obtained from the FCM were classified based on the LST and NDVI values and divided into nine classes; the first class represents the clusters that have a high degree of LST and a low level of NDVI; on the contrary, class 9 groups the clusters that record the lowest LST value and the highest degree of NDVI. The classification result is shown in Figure 7.

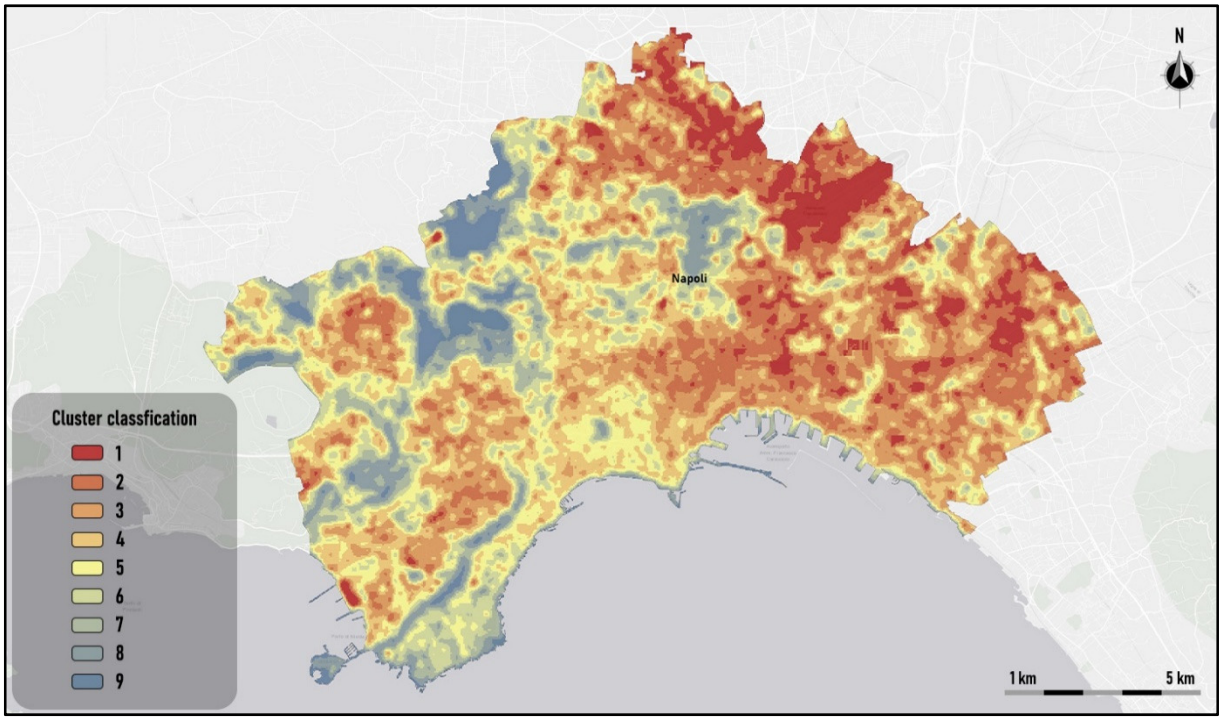

Figure 7. Thematic map of the FCM's output classification.

Following the classification of the FCM results and based on the hot and cold thresholds shown in Figure 6, the clusters that constitute cold and hot spots were identified. The polygons belonging to the clusters that exceed the cold threshold (9, 1, and 8, in turn reclassified as 9, 8, and 7) were grouped to determine the cold spots of the study area; similarly, the polygons belonging to the clusters that are below the hot threshold (3, 4, and 6, in turn reclassified as 3, 2, and 1) were grouped to determine the hotspots of the study area. The hot and cold spot detection result is shown in Figure 8.

The thematic map delineates a pronounced prevalence and spatial distribution of cold spots in the northwestern and western regions of the study area. This pattern is primarily attributable to the substantial presence of green spaces in these zones, where vegetation plays a critical role in modulating ambient temperatures and inhibiting the formation of UHIs. The inverse is evident in the prominent hotspot extending from the central to the eastern periphery of the study area. This zone is typified by a dense urban fabric, extensive industrial complexes, and a notable scarcity of vegetation, all of which contribute to the intensification of heat.

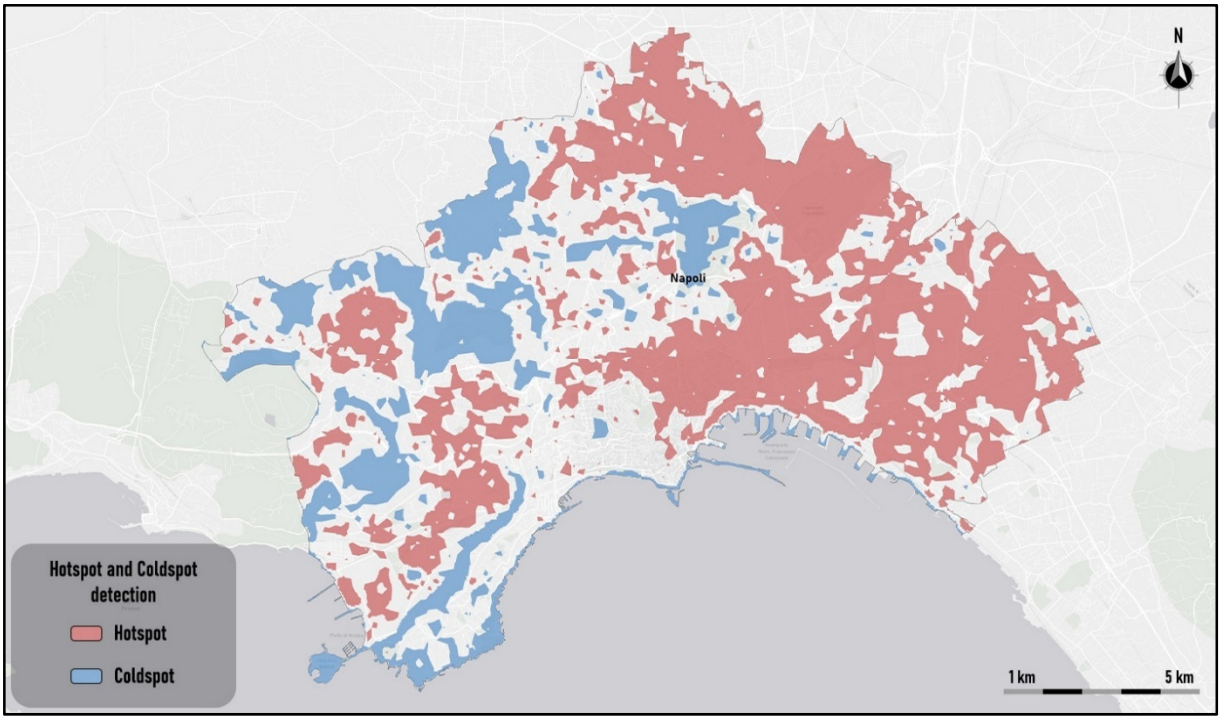

Figure 8. Hotspot and Coldspot detection.

The northern region constitutes an anomaly in this context, as it, despite being characterized by an abundance of medium-sized green spaces, represents a significant hotspot. This localized thermal anomaly may be attributed to the specific nature of the greenery present. Unlike the western sector, which predominantly features shrubland and woodland vegetation types, the northern area is primarily dominated by urban green spaces, such as decorative flowerbeds, which lack the substantial canopy cover provided by medium to large trees. Consequently, these urban greenspaces may offer insufficient thermal mitigation compared to more substantial, natural vegetation types.

Finally, a reliability analysis was performed to measure the average value of the maximum membership degree of each hotspot; three classes were created based on the value of the membership degree: *Low, Medium,* and *High.* The *Low* class groups hotspots with a degree lower than 0.50; the Medium class contains hotspots with a degree equal to or greater than 0.50 and less than 0.75; and the *High* class includes hotspots with a degree equal to or greater than 0.75. The spatial distribution of the reliability classes is shown in the thematic map in Figure 9.

The areas to the north and east of the study area exhibit the most extensive UHIs. As previously mentioned, the causes are to be found in the typology of the urban fabric that characterizes these areas, predominantly devoid of green spaces but rich in impermeable surfaces.

Evaluating the reliability of each hotspot, it is possible to note that the vast majority of the UHIs identified have a *High* value. Table 1 shows the percentages of UHI areas divided into reliability classes calculated with respect to their overall surface.

Table 1. Percentage distribution of the average reliability classes of UHIs.

Reliability Class	Area [km^2]	Percentage
High	43.87	94.26%
Medium	2.62	5.63%
Low	0.05	0.11%

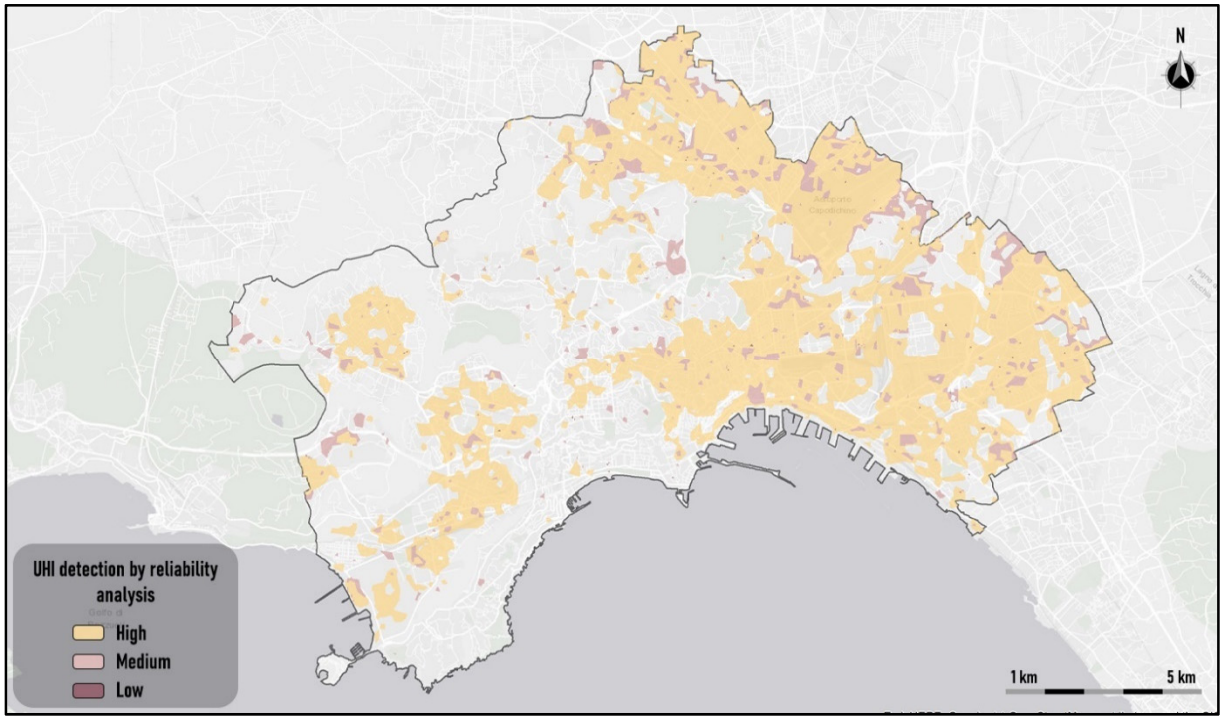

Figure 9. Thematic map of UHI detection by reliability analysis.

The sum of the UHI areas amounts to 46.54 km^2 and represents 39.92% of the entire study area, which measures 118.38 km^2.

About 95% of these UHIs have a reliability of High, which exceeds 0.75.

These results show that most of the urban areas of the city of Naples identified as UHIs can be considered UHIs with a high level of reliability. This imply that the proposed method provides a good reliability level for the UHIs detected.

To test the accuracy of the obtained results, the detected UHIs were compared with those obtained by applying the UHI detection method in [29], where a sampling interval of 10 m was used and the number of classes was fixed to seven.

The sum of the UHI areas detected by employing this UHI detection method [29] was 42.97 km^2, representing 36.30% of the area of the city.

About 95.75% of the UHIs detected using the proposed method were covered by UHIs detected using the method [29]. Table 2 shows the percentage of UHIs with *High*, *Medium*, and *Low* reliability that are covered by UHIs detected using the method of [29].

Table 2. Percentage of UHIs covered by UHIs detected executing the algorithm of [29].

Reliability Class	Area [km^2]	Percentage of Area Covered by UHIs Obtained Using [29]
High	43.87	97.02%
Medium	2.62	75.16%
Low	0.05	57.68%

The results in Table 2 show that over 97% of UHIs classified as High reliability are covered by UHIs detected using the method of [29]. This highlights that the proposed UHI detection method provides accurate results and, unlike other clustering-based UHI detection algorithms, provides an effective estimate of their reliability.

5.2. Final Discussion

From the knowledge of the study area, its morphology, and the connotation of the soil typologies, it emerges that the UHI detection model provides high accuracy in the localization of UHIs. In fact, the determined hotspots cover urban areas characterized mainly by impermeable materials and with high building density. On the contrary, the cold spots cover urban areas rich in permeable green surfaces with high vegetative vigor. A further benefit of the model is constituted by the assessment of the reliability of the UHIs detected.

The majority of the detected UHI areas have high reliability and, in comparisons made with the model in [29], almost all the UHIs with high reliability are covered by UHIs detected executing the model [29]. The main limitation of the model is constituted by the low resolution of the satellite LST data, equal to 30 m $\times$ 30 m, which affects the precision of the localization of UHIs at an urban scale. To obtain a higher resolution, it would be necessary to integrate the satellite data with on-the-ground measurements of the LST; however, acquiring on-the-ground measurements at high spatial resolution would require high costs and acquisition times.

6. Conclusions

A new GIS-based framework designed to detect UHIs and identify the most critical urban areas during heatwave events is proposed. This approach applies the FCM algorithm with remotely sensed LST and NDVI data to detect and assess the spatial distribution of UHIs, where the optimal number of clusters is determined using well-known validity indices. To assess the reliability of a potential urban hotspot and confirm its identification as a UHI, a reliability index is computed.

The study was carried out within the urban framework of Naples, Italy, chosen for its notable attributes of elevated population density and significant urban development.

The application of the FCM algorithm, known for its computational efficiency, enables the proposed methodology to be effectively applied to remotely sensed imagery. Furthermore, the use of various validity indices allows for the determination of the optimal number of clusters, even in the presence of noise in the data. An additional advantage of the proposed UHI detection method is the assessment of the reliability of UHIs, which represents a quantitative measure of the accuracy of the results and provides, in contrast to other UHI detection approaches, a decision support tool for assessing the accuracy of UHIs.

A primary limitation of the proposed method lies in the relatively low resolution of the LST raster derived from satellite-based thermal imagery. To potentially enhance the spatial resolution of the LST dataset, the use of thermal cameras mounted on drones could be considered. However, this would necessitate the deployment of specialized equipment and costly data collection campaigns to comprehensively cover the entire urban area, with the added challenge of the duration of such efforts potentially exceeding that of the heatwave event itself.

Future research will focus on further improving the precision of this detection method and conducting additional experiments across different urban environments and heatwave scenarios. In particular, the framework will be integrated with heatwave vulnerability and impact/risk models to provide decision makers with a comprehensive tool to support the assessment of adaptation strategies in UHIs with high risks/impacts for residents' health. Finally, this work can be addressed in future multidisciplinary research in which the results will be further explored at a detailed scale with on-the-ground measurements, and the contribution of urban analysis and planning specialists will be necessary to assess optimal mitigation strategies and to evaluate the costs of the planned actions.

Author Contributions: Conceptualization, R.C., B.C., V.D., F.D.M. and V.M.; methodology, R.C., B.C., V.D., F.D.M. and V.M.; software, R.C., B.C., V.D., F.D.M. and V.M.; validation, R.C., B.C., V.D., F.D.M. and V.M.; formal analysis, R.C., B.C., V.D., F.D.M. and V.M.; investigation, R.C., B.C., V.D., F.D.M. and V.M.; resources, R.C., B.C., V.D., F.D.M. and V.M.; data curation, R.C., B.C., V.D., F.D.M. and V.M.; writing—original draft preparation, R.C., B.C., V.D., F.D.M. and V.M.; writing—review and editing, R.C., B.C., V.D., F.D.M. and V.M.; visualization, R.C., B.C., V.D., F.D.M. and V.M.; supervision, R.C., B.C., V.D., F.D.M. and V.M. All authors have read and agreed to the published version of the manuscript.

Funding: This research received no external funding.

Data Availability Statement: The data presented in this study are available on request from the corresponding author.

Acknowledgments: This study was carried out within the RETURN Extended Partnership and received funding from the European Union Next-GenerationEU (National Recovery and Resilience Plan—NRRP, Mission 4, Component 2, Investment 1.3—D.D. 1243 2/8/2022, PE0000005.

Conflicts of Interest: The authors declare no conflicts of interest.

References

1. Jabbar, H.K.; Hamoodi, M.N.; Al-Hameedawi, A.N. Urban heat islands: A review of contributing factors, effects and data. *IOP Conf. Ser. Earth Environ. Sci.* **2023**, *1129*, 012038. [CrossRef]
2. Singh, C.; Ramesh, A.; Hagenlocher, M.; Shekhar, H.; Siemons, A.S.S.; Okunola, O.H.; Werners, S.E. Applying recent advances in climate adaptation research to urban heat risk management. *WIREs Clim. Change* **2024**, *15*, e901. [CrossRef]
3. Lemonsu, A.; Lemonsu, A.; Alessandrini, J.M.; Capo, J.; Claeys, M.; Cordeau, E.; de Munck, C.; Dahech, S.; Dupont, J.C.; Dugay, F.; et al. The Heat and Health in Cities (H2C) project to support the prevention of extreme heat in cities. In Proceedings of the EMS Annual Meeting 2024, Barcelona, Spain, 1–6 September 2024; EMS2024-982. [CrossRef]
4. MacLachlan, A.; Biggs, E.; Roberts, G.; Boruff, B. Urbanisation-Induced Land Cover Temperature Dynamics for Sustainable Future Urban Heat Island Mitigation. *Urban Sci.* **2017**, *1*, 38. [CrossRef]
5. Pierre, T.J.; Rahman, M.M.; Amin, M.A.; Munshi, M. Deciphering Urban Footprints on Climate Variability through an Innovative Inquiry into Heat Island Phenomena. *FMDB Trans. Sustain. Appl. Sci.* **2024**, *1*, 34–43. [CrossRef]
6. Huang, W.T.K.; Masselot, P.; Bou-Zeid, E.; Fatichi, S.; Paschalis, A.; Sun, T.; Gasparrini, A.; Manoli, G. Economic valuation of temperature-related mortality attributed to urban heat islands in European cities. *Nat. Commun.* **2023**, *14*, 7438. [CrossRef] [PubMed]
7. Huang, H.; Zhao, Y.; Deng, X.; Yang, H.; Ren, L. Health risk appraisal of urban thermal environment and characteristic analysis on vulnerable populations. *J. Environ. Eng. Landsc. Manag.* **2023**, *31*, 34–43. [CrossRef]
8. Stewart, I.D.; Oke, T.R. Local Climate Zones for Urban Temperature Studies. *Bull. Am. Meteorol. Soc.* **2012**, *93*, 1879–1900. [CrossRef]
9. Voogt, J.A.; Oke, T.R. Thermal remote sensing of urban climates. *Remote Sens. Environ.* **2003**, *86*, 370–384. [CrossRef]
10. Mostovoy, G.V.; King, R.L.; Reddy, K.R.; Kakani, V.G.; Filippova, M.G. Statistical estimation of daily maximum and minimum air temperatures from MODIS LST data over the state of Mississippi. *GIScience Remote Sens.* **2006**, *43*, 78–110. [CrossRef]
11. Prihodko, L.; Goward, S.N. Estimation of air temperature from remotely sensed sur-face observations. *Remote Sens. Environ.* **1997**, *60*, 335–346. [CrossRef]
12. Zhang, P.; Imhoff, M.L.; Wolfe, R.E.; Bounoua, L. Characterizing urban heat islands of global settlements using MODIS and nighttime lights products. *Can. J. Remote Sens.* **2010**, *36*, 185–196. [CrossRef]
13. Peng, S.; Piao, S.; Ciais, P.; Friedlingstein, P.; Ottle, C.; Breon, F.M.; Myneni, R.B. Surface urban heat island across 419 global big cities. *Environ. Sci. Technol.* **2012**, *46*, 696–703. [CrossRef]
14. Yating, H.; Chuncheng, Z.; Yang, Y.; Fuheng, Q. A cluster validity index for fuzzy c-means clustering. In Proceedings of the 2011 International Conference on System science, Engineering design and Manufacturing informatization, Guiyang, China, 22–23 October 2011; pp. 263–266. [CrossRef]
15. Johari, F.; Peronato, G.; Sadeghian, P.; Zhao, X.; Widén, J. Urban building energy modeling: State of the art and future prospects. *Renew. Sustain. Energy Rev.* **2020**, *128*, 109902. [CrossRef]
16. Biljecki, F.; Chew, L.Z.X.; Milojevic-Dupont, N.; Creutzig, F. Open government geospatial data on buildings for planning sustainable and resilient cities. *arXiv* **2021**, arXiv:2107.04023. [CrossRef]

17. Lipson, M.; Nazarian, N.; Hart, M.A.; Nice, K.A.; Conroy, B. A transformation in city-descriptive input data for urban climate models. *Front. Environ. Sci.* **2022**, *10*, 866398. [CrossRef]
18. Boccalatte, A.; Thebault, M.; Menezo, C.; Ramousse, J.; Fossa, M. Evaluating the impact of urban morphology on rooftop solar radiation: A new city-scale approach based on Geneva GIS data. *Energy Build.* **2022**, *260*, 111919. [CrossRef]
19. D'Acci, L.; Batty, M. The Mathematics of Urban Morphology. In *Modeling and Simulation in Science, Engineering and Technology*; Springer International Publishing: Berlin/Heidelberg, Germany, 2019; pp. 352–355. [CrossRef]
20. Tardioli, G.; Kerrigan, R.; Oates, M.; O'Donnell, J.; Finn, D.P. Identification of representative buildings and building groups in urban datasets using a novel preprocessing, classification, clustering and predictive modelling approach. *Build. Environ.* **2018**, *140*, 90–106. [CrossRef]
21. Fleischmann, M.; Feliciotti, A.; Kerr, W. Evolution of urban patterns: Urban morphology as an open reproducible data science. *Geogr. Anal.* **2021**, *54*, 536–558. [CrossRef]
22. Maiullari, D.; Pijpers-Van Esch, M.; van Timmeren, A. A quantitative morphological method for mapping local climate types. *Urban Plan.* **2021**, *6*, 240–257. [CrossRef]
23. Kwak, Y.; Park, C.; Deal, B. Discerning the success of sustainable planning: A comparative analysis of urban heat island dynamics in Korean new towns. *Sustain. Cities Soc.* **2020**, *61*, 13. [CrossRef]
24. Mejía-Parada, C.; Mora-Ruiz, V.; Soto-Paz, J.; Parra-Orobio, B.A.; Attia, S. Microclimate Zoning Based on Double Clustering Method for Humid Climates with Altitudinal Gradient Variations: A Case Study of Colombia. *Atmosphere* **2024**, *15*, 709. [CrossRef]
25. Arandin, N.; Arabi, M.; Jahdi, R. Modeling and Evaluation of Effective Factors on thermal islands with an approach based on fuzzy systems: A case study of Tehran. *Res. Sq.* 2023, *preprint* (Version 1); 28p. [CrossRef]
26. Acosta, M.P.; Vahdatikhaki, F.; Santos, J.; Patricia, S.; Andries, J.; Doree, G. Data-driven Analysis of Urban Heat Island Phenomenon Based on Street Typology. *Sustain. Cities Soc.* **2023**, *101*, 17. [CrossRef]
27. Wang, D.; Zhang, B. An urban heat island functional zoning approach based on weighted kernel K-means. In Proceedings of the SPIE 12815, International Conference on Remote Sensing, Mapping, and Geographic Systems (RSMG 2023), Kaifeng, China, 7–9 July 2023. [CrossRef]
28. Doan, Q.V.; Amagasa, T.; Pham, T.H.; Sato, T.; Chen, F.; Kusaka, H. Novel clustering framework using k-means (S k-means) for mining spatiotemporal structured climate data. *Geosci. Model Dev.* **2022**, *16*, 32. [CrossRef]
29. Cafaro, R.; Cardone, B.; D'Ambrosio, V.; Di Martino, F.; Miraglia, V. A New GIS-Based Framework to Detect Urban Heat Islands and Its Application on the City of Naples (Italy). *Land* **2024**, *13*, 1253. [CrossRef]
30. Sowmya, B.; Sheelarani, B. Land cover classification using reformed fuzzy C-means. *Sadhana* **2011**, *36*, 153–165. [CrossRef]
31. Dinh Sinh, M.; Long Thanh, N. Semi-supervised fuzzy C-means clustering for change detection from multispectral satellite image. In Proceedings of the 2015 IEEE International Conference on Fuzzy Systems (FUZZ-IEEE), Istanbul, Turkey, 2–5 August 2015; pp. 1–8. [CrossRef]
32. Cardone, B.; Di Martino, F.; Miraglia, V. A GIS-Based Fuzzy Model to Detect Critical Polluted Urban Areas in Presence of Heatwave Scenarios. *Computers* **2024**, *13*, 143. [CrossRef]
33. Cardone, B.; Cerreta, M.; Di Martino, F.; Miraglia, V.; Sacco, S. A fuzzy-based emotion detection method to classify the attractiveness of urban green spaces. *Evol. Intell.* **2024**, *17*, 3921–3933. [CrossRef]
34. Bezdek, J.C. *Pattern Recognition with Fuzzy Objective Function Algorithms*; Kluwer Academic Publishers: Norwell, MA, USA, 1981; p. 256. [CrossRef]
35. Bezdek, J.C.; Ehrlich, R.; Full, W. FCM: The fuzzy c-means clustering algorithm. *Comput. Geosci.* **1984**, *10*, 191–203. [CrossRef]
36. Xie, X.L.; Beni, I.G. A validity measure for fuzzy clustering. *IEEE Trans. Pattern Anal. Mach. Intell.* **1991**, *13*, 841–847. [CrossRef]
37. Davies, D.L.; Bouldin, D.W. A cluster separation measure. *IEEE Trans. Pattern Anal. Mach. Intell.* **1979**, *1*, 224–227. [CrossRef] [PubMed]
38. Fukuyama, Y.; Sugeno, M. A new method of choosing the number of clusters for the fuzzy C-means method. In Proceedings of the fifth Fuzzy System Symposium, New Orleans, LA, USA, 11 September 1996; pp. 247–250. [CrossRef]
39. Todeschini, R.; Ballabio, D.; Termopoli, V.; Consonni, V. Extended multivariate comparison of 68 cluster validity indices. A review. *Chemom. Intell. Lab. Syst.* **2024**, *251*, 105117. [CrossRef]